nature ecology & evolution

ARTICLES

https://doi.org/10.1038/s41559-019-1008-x

Information limitation and the dynamics of coupled ecological systems

Andrew M. Hein[1,2*] and Benjamin T. Martin[1,2,3]

The dynamics of large ecological systems result from vast numbers of interactions between individual organisms. Here, we develop mathematical theory to show that the rate of such interactions is inherently limited by the ability of organisms to gain information about one another. This phenomenon, which we call 'information limitation', is likely to be widespread in real ecological systems and can dictate both the rates of ecological interactions and long-run dynamics of interacting populations. We show how information limitation leads to sigmoid interaction rate functions that can stabilize antagonistic interactions and destabilize mutualistic ones; as a species or type becomes rare, information on its whereabouts also becomes rare, weakening coupling with consumers, pathogens and mutualists. This can facilitate persistence of consumer–resource systems, alter the course of pathogen infections within a host and enhance the rates of oceanic productivity and carbon export. Our findings may shed light on phenomena in many living systems where information drives interactions.

Coupled population models are used to study immune function[1], disease epidemics[2], plant–pollinator networks[3], food web dynamics[4], oceanic nutrient cycling[5] and a host of other important biological phenomena. A defining feature of these and many other living systems is that interactions among populations emerge from individual organisms perceiving and actively locating one another using sensory information[6,7]. This behaviour causes the motion of one organism to become correlated with the location of another over distances that can range from a few to thousands of body lengths[8–10]. In the most widely used mean-field models of ecological interactions, these correlations are assumed to be either very short-range or weak, such that mass action provides a reasonable description of ecological interaction rates[11–14]. Here, we explicitly incorporate these information-induced correlations into a more general model of ecological interactions. By building on stochastic reaction rate theory[15,16], our framework integrates responses to sensory information by deriving long-run interaction rates from observed movement characteristics of individual organisms. The framework can readily be applied to empirical data to relate empirical patterns of movement to long-run interaction rates (see 'Estimating model parameters from data' in Supplementary Discussion). Our analysis reveals two important findings. First, our model shows that the kinds of responses to sensory information that are empirically observed in ecological systems[7] can have a dominant effect on interaction rates, determining both the value of the interaction rate and the functional form that relates interaction rate to population densities. Second, our analysis reveals that the dynamical properties of interacting populations, including stability, oscillations and rates of productivity, depend intimately on the way organisms respond to sensory information. Our theory provides a mathematical framework for connecting sensory information and behaviour at the organismal level to the long-run dynamics of interacting populations.

Results

To derive interaction rates, we consider interactions between a 'searcher' population (predator, disease vector, pollinator or immune cell) and a 'target' population (prey, host, flower or pathogen, Fig. 1a). Searchers move through the environment at speed v and interact with targets (for example, by attacking prey) when they come within a short interaction distance, l_i. We incorporate responses to sensory information by considering targets that produce a signal. Signals are ubiquitous in living systems and are produced both actively[17,18]—as in the case of acoustic calls or visual displays—and passively, such as through excretion of metabolic waste (for example, carbon dioxide[12,19]) or sound production during feeding or locomotion[8] (Fig. 1b). Searchers use such signals to navigate to targets[7,12,19,20], typically by biasing motion towards the target when the signal is sufficiently strong (Fig. 1c). We define l_* as the distance within which the searcher gains information about a target's location via signals and biases its motion accordingly (Fig. 1a).

When targets are sparse, the typical distance from a searcher to the nearest target is large and searchers primarily move through space at random with respect to targets (Fig. 2a). As density increases, the fraction of space within a distance l_* of a target increases sharply (Fig. 2a, insets), and searcher motion becomes directed towards targets throughout much of the environment. The important point is this: the typical movement pattern of searchers in an environment with sparse targets is qualitatively different from typical searcher movements when targets are dense (Fig. 2a, curve). To understand the effect this transition from primarily random to primarily directed motion has on interaction rate, λ, we begin by deriving interaction rates for the two extremes: purely random motion and purely directed motion (Fig. 2b, red line and black curve, respectively). When searchers move at random everywhere in the environment, interaction rate is linear or near linear in target density (Fig. 2b, red line) as in conventional mass action-based models of ecological interactions[11,13,14]. On the contrary, when motion is directed towards targets everywhere, interaction rates are determined by the time taken to move directly from one target to the next. In a uniform random target field or lattice, the typical distance to a target is proportional to $\rho^{-1/n}$, leading to the low density (that

[1]Institute of Marine Sciences, University of California Santa Cruz, Santa Cruz, CA, USA. [2]National Oceanic and Atmospheric Administration, Southwest Fisheries Science Center, Santa Cruz, CA, USA. [3]Institute for Biodiversity and Ecosystem Dynamics, University of Amsterdam, Amsterdam, the Netherlands. *e-mail: andrew.hein@noaa.gov

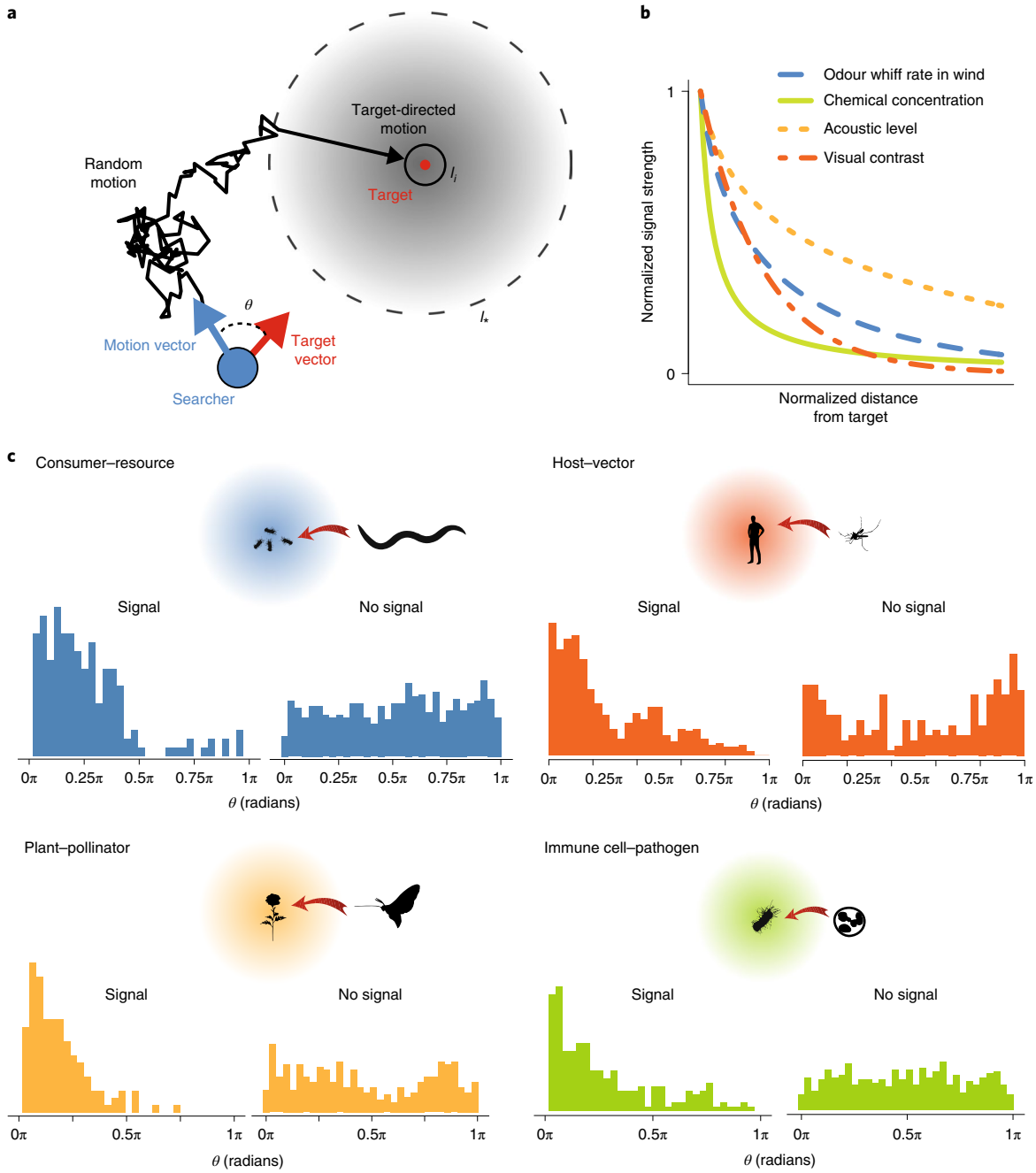

Fig. 1 | Model setup, sensory signals and searcher motion in empirical systems. a, Searcher moves through target landscape. Turns are uniform random when distance is greater than l_*, and biased towards the target when distance is less than l_*. **b**, Normalized signal strength (signal strength/strength at source) as function of distance from source for chemical gradient produced by a point source in still water[12] (green), acoustic level from a sound source[52] (yellow), rate of odour whiffs downwind of a scent source[53] (blue) and object–background visual contrast in water[33] (orange). Signals decay with distance leading to finite detection length scale, l_*. **c**, Effect of sensory signals on movement behaviour of nematode, *Caenorhabditis elegans*, in search of prey[54]; mosquito, *Aedes aegypti*, in search of CO_2 source[19,55]; moth, *Manduca sexta*, in presence and absence of plant volatiles[56]; and immune cells (neutrophils) in absence of wound (right) and in the vicinity of a wound site[20] (left). 'Signal' histograms show distribution of angle, θ, in experiments where a sensory signal was provided. 'No signal' histograms are from experiments where the signal was absent.

is, $\rho \ll l_i^{-2}$) scaling, $\lambda \propto \rho^{\frac{1}{n}}$ (Fig. 2b, black curve and Supplementary Discussion), where n is the dimension of the environment, ρ is target density and λ is the rate of interactions between the searcher and targets[14]. At high densities, both random and directed searches become limited by interaction duration (that is, handling time), h, rather than search time and the interaction rate in both models approaches $1/h$.

The limits of purely random motion and purely directed motion (Fig. 2b) form an envelope within which real biological systems operate. For any finite value of the sensory length scale, $l_* > l_i$, the interaction rate between searchers and targets is determined by a mixture of random and directed motion (Fig. 2a). In particular, the long-run interaction rate is $\lambda = (\langle \tau \rangle + h)^{-1}$, where h is the duration of each interaction (that is, handling time),

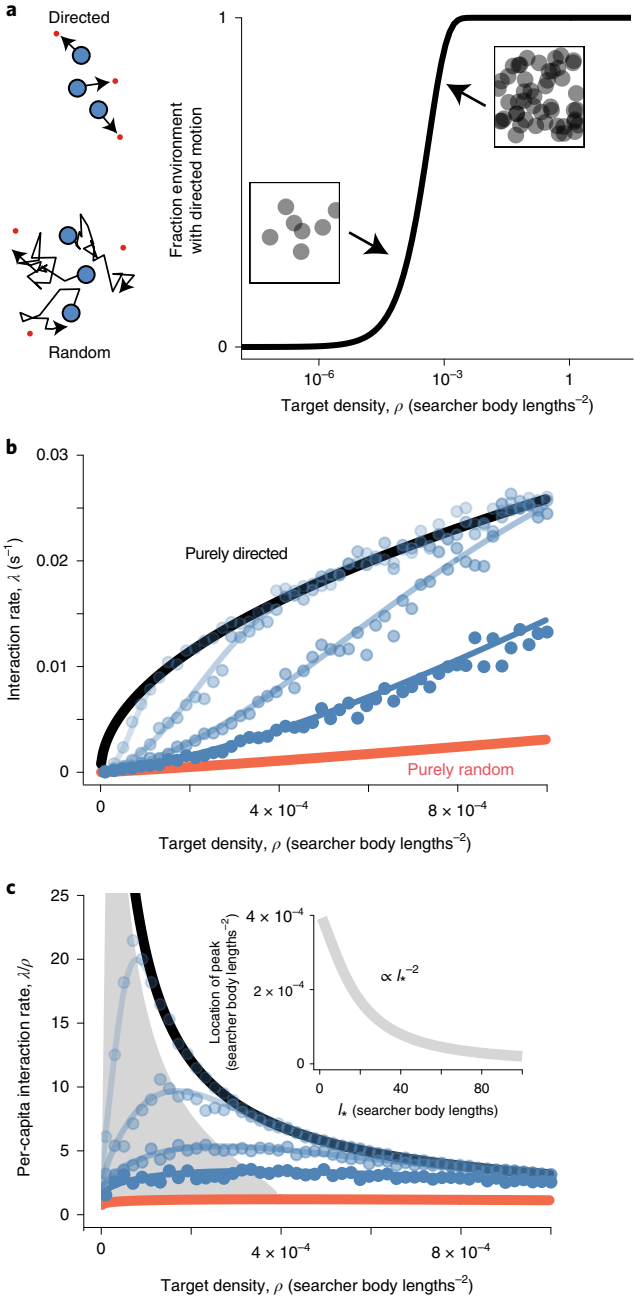

Fig. 2 | Information, motion and interaction rates. a, Searcher motion changes qualitatively with changing target density. Motion is primarily random when targets are sparse and directed when targets are dense. **b**, Rate of interactions between searcher and targets across a range of target density. Limiting cases of purely random motion (red line) and purely directed motion (black line) provide bounds on performance when detection length, l_*, is finite (blue curves). Note the sigmoid shape of blue curves. Different curves show different values of l_*, from high (light blue) to low (dark blue). Curves are generated by solving for λ as described in Methods, assuming diffusive motion in region $l > l_*$ and $h = 0$ (see Supplementary Table 1 for parameter values). Points are mean encounter rates generated from 100 replicate individual-based simulations of searcher–target interactions. **c**, Per-capita interaction rates for curves shown in **b** with $h = 300$ s. When l_* is finite (blue curves), per-capita rate increases at low density before decreasing at high density, indicating a lower regime where information is limiting (grey region) and an upper regime where the time per interaction (that is, handling time) is limiting. Location of peak per-capita interaction rate (grey region) demarcates these regimes. Peak location is determined by sensory length scale, l_* (inset).

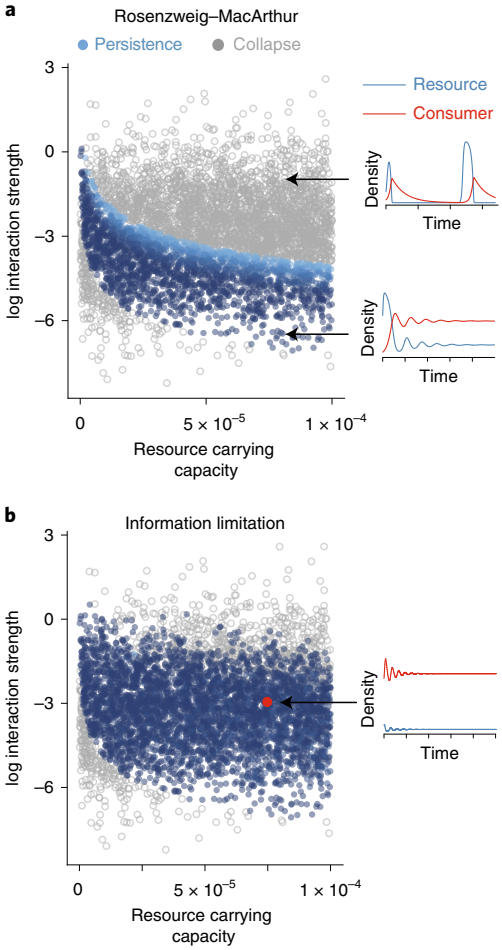

Fig. 3 | Population persistence and collapse in consumer–resource systems. Each point represents a consumer–resource system (Rosenzweig–MacArthur model) with parameters chosen at random from empirically derived ranges[23,24] (see Methods and Supplementary Discussion). **a**,**b**, Point colour indicates population persistence (blue) or collapse (grey) when interactions are governed by a type II functional response (**a**) or information-limited interactions (**b**) (Methods, equation (1)). Note that increasing carrying capacity lowers the upper limit of interaction strengths where persistence is possible in **a**, but not in **b**. Point hue indicates amplitude of prey cycles for persisting populations: small amplitude (dark blue) and large amplitude (light blue). Insets show example time series. Systems were considered to collapse if either population density fell below 10^{-20}.

and τ is mean search time. Mean search time can be written $\langle\tau\rangle = \int_{l_*}^{\infty} p(l)\tau_{\text{random}}(l)\mathrm{d}l + \int_{0}^{\infty} p(l)\tau_{\text{directed}}\mathrm{d}l$, where $p(l)$ is the probability that a searcher begins its search a distance, l, from the nearest target, τ_{random} is the mean time taken to reach l_* by random motion from a distance $l > l_*$, and τ_{directed} is the time taken to move directly to the target within the region of directed motion. In Methods, we show how this formulation can be used to derive the interaction rate, λ, from the properties of searcher motion and the sensory length scale, l_* (see Methods, equation (1)). Using our framework, the interaction rate function in any given empirical system can be derived directly from behavioural data by empirically estimating model parameters (Supplementary Discussion).

For a wide range of biophysically constrained assumptions (see Methods, Supplementary Discussion and Extended Data Figs. 1–3), the interaction rate between searchers and targets is a sigmoid function that transitions from being approximately linear in target density when density is low, to super-linear and eventually saturating

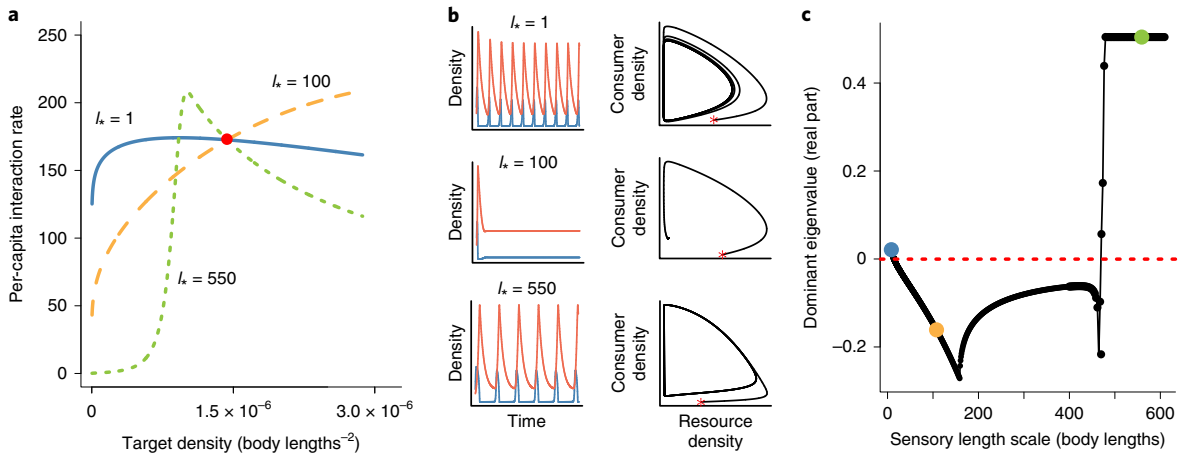

Fig. 4 | Information limitation dictates qualitative dynamics in consumer–resource systems. a, Per-capita interaction rate function of the consumer–resource system with information limited interactions shown in Fig. 3b (red point) for three different values of sensory length scale, l_*. Curves are scaled by adjusting searcher speed, v, so all three have the same interaction rate at equilibrium (red circle), but the shape of curves for low (blue solid line), intermediate (orange dashed line) and high l_* (green dotted line) differ. **b**, Time series (left) and phase portraits (right) for consumer–resource systems with per-capita interaction rates shown in **a**. **c**, Dominant eigenvalue of the Jacobian matrix of consumer–resource system at equilibrium across a range of values of l_*. Point colours indicate corresponding curves in **a**. Note positive eigenvalue for very small and very large values of l_*, indicating the loss of a stable fixed point at these extremes.

at high target density (Fig. 2b, blue curves). This transition occurs because, as density increases, searchers transition from spending most of their time in undirected search to spending most of their time moving directly towards targets (Fig. 2a). In analogy with diffusion-limited chemical reactions[15,16], we refer to the regime where the contribution of random motion dominates the interaction rate as the 'information limited' regime.

An important implication of the sigmoid interaction rate functions shown in Fig. 2b is that the efficiency of searchers varies systematically with the density of targets (Fig. 2c). The per-capita risk of a given target being found by a searcher initially increases as density increases, before decreasing at higher densities; the rate of interactions transitions from being information-limited at low target density (Fig. 2c, grey region) to handling time-limited at high density. We explore the population dynamic consequences of this non-monotonic risk[21], and of information limitation more generally, using four types of widely used ecological models: consumer–resource models, models of interacting mutualists, immune cell–pathogen models and models of biomass flux in patchy environments.

Classical consumer–resource models in which the resource grows logistically and the consumer and resource interact via saturating mass action kinetics (that is, type II functional response) exhibit a peculiar feature known as the 'paradox of enrichment': when the carrying capacity of the resource is high, both resource and consumer populations begin to oscillate. Oscillations increase in amplitude until extinctions of finite populations occur[22]. Using empirically derived parameters[23,24] (see Supplementary Discussion) we find that under standard coupled population models, large amplitude cycles lead to the collapse of consumer–resource systems over a wide range of biologically relevant parameter space (Fig. 3a, grey points indicate collapsing communities). If the type II functional response is replaced by an information-limited interaction rate (that is, Fig. 2b, blue curves; Methods equation (1)), the region over which consumer–resource systems persist expands significantly (Fig. 3b, blue points indicate persisting communities). This enhanced persistence follows from the reduced efficiency of consumers at low resource densities[21] captured by the information-limited model (Fig. 2c); once the resource becomes rare enough, information-limited consumers are unable to drive the resource to lower densities.

Because it expresses demographic parameters as functions of organismal-level traits, our framework allows one to predict how changes in consumer and resource traits affect demography. For example, conditioning on a fixed value of the interaction rate at equilibrium (Fig. 4a, red point), whether the consumer–resource system exhibits a stable fixed point or a limit cycle hinges on the value of the sensory length scale, l_*. When l_* is either very small or very large, the inflection point of the interaction rate function occurs below the equilibrium resource density, and dynamics become unstable (Fig. 4a,b, upper and lower panels). However, for intermediate values of l_*, the inflection point of the interaction rate occurs above equilibrium resource density, such that resource risk decreases as resource density decreases (Fig. 4a, orange dashed line). This leads to a stable consumer–resource equilibrium (Fig. 4b, middle panel). The effect of the sensory length scale on stability can be seen in more general terms by plotting the dominant eigenvalue of the Jacobian matrix of the consumer–resource system at equilibrium (Fig. 4c), which indicates a large region of stable dynamics for intermediate l_*.

The non-monotonic change in per-capita interaction rates with density predicted by our model follows from the sigmoid shape of the information-limited interaction rate function (Fig. 2b). Sigmoid interaction rate functions—for example, type III functional responses[25–27]—are widely used in food web models, in part because they are known to stabilize large oscillations[28] that seldom occur in real systems[29]. The sigmoid form has typically been attributed to complex behaviours such as adaptive prey switching[25] or very specific forms of learning[26]. However, our model reveals that a sigmoid form can emerge from the much more general constraint of limited information about the locations of targets illustrated in Fig. 2. Our results, therefore, suggest that information limitation could help to explain the origin of sigmoid interaction rate functions in empirical systems[27] and, as a result, the rarity of large amplitude cycles in real food webs[29]. Despite having a similar shape, our model is not mathematically equivalent to a type III functional response; we will return to this point and to its theoretical implications for bridging organismal and population levels of organization in the Discussion.

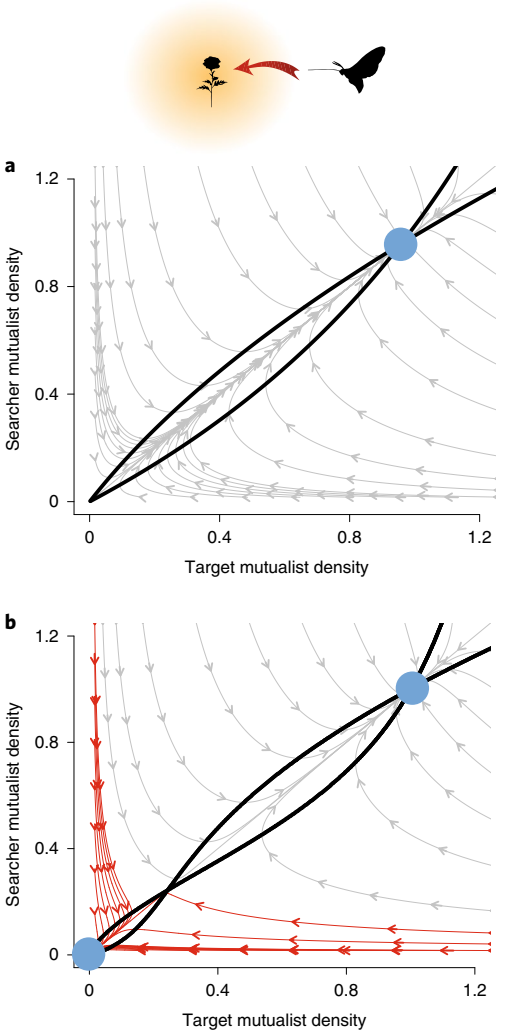

Fig. 5 | Information limitation can destabilize mutualistic interactions. **a**,**b**, Null clines (thick black lines) and stable equilibria (blue points) for obligate mutualist species under a standard type II functional response (**a**) and information limitation (**b**). Weakened coupling under information limitation causes system collapse when either population density is too low (red lines in **b**; see Methods). Shown is a case where populations grow logistically with carrying capacity of zero in the absence of the other population.

In contrast to their stabilizing effect on antagonistic interactions, the weakened interaction rates at low density that occur under information limitation can destabilize the dynamics of interacting mutualists by introducing or expanding a basin of attraction that leads to population collapse (compare Fig. 5a,b). This effect follows intuitively from the fact that, under information limitation, the per-capita rate at which searchers encounter targets becomes very low as target density becomes low, because searchers lack sufficient information to find targets quickly. Both mutualists suffer in this regime and populations cannot be sustained.

The key feature of our framework (Figs. 1 and 2) is that it relates measurable, micro-scale features of ecological interactions—for example, patterns of searcher motion and responses to sensory signals (Fig. 1c)—to long-run interaction rates. It is, therefore, particularly useful for studying dynamics of systems in which micro-scale behaviour is easy to measure but population dynamics are difficult to anticipate. An example is the within-host dynamics of pathogen infections. Classic models of infections assume immune cell–pathogen encounters are governed by mass action[1,30]. However, many immune cell types actively locate infection sites using chemotaxis[20,31] (Fig. 1c), which suggests cells interact with pathogens through a mixture of undirected and directed motion (Fig. 2a). We parameterized our model (see Methods) using empirical responses of immune cells to a localized wound site[18]. Because of the same mechanism that stabilizes consumer–resource interactions (Fig. 3a), the model predicts that rare pathogens can persist at low levels in the body without being eradicated over a far wider range of conditions than conventional models suggest[1,30]. Moreover, our model can predict how the disruption of chemotaxis that occurs during systemic infections[31] erodes the ability of host immune cells to control infections. If the length scale over which immune cells detect infections sites is reduced during the course of the infection[31], these cells can lose the ability to locate infection sites, leading to uncontrolled proliferation of the pathogen (Fig. 6a).

Our theoretical framework extends readily to spatially patchy ecological systems that are not well described by existing mean-field ecological theory. For example, in marine ecosystems, trophic interactions are concentrated in highly productive 'hotspots'[5] (Fig. 6b). Recruitment of marine consumers to hotspots is well documented[32], but has only recently been included in marine ecosystem models, typically through individual-based simulations or empirically parameterized covariance between consumer and resource densities[5]. Our model provides an intermediary between these parameter-heavy, spatial population models and conventional mean-field models that ignore structure in the environment. We applied the model to a population of marine predators (for example, sea birds and salmon) that move through the environment following the dynamic shown in Fig. 1a, where a 'target' is now a productivity hotspot and l_* is the detection length scale for signals produced at the hotspot (for example, wind-borne dimethyl sulfide[32]). The ability of marine predators to exploit hotspots depends on the length scale l_*. This length scale, in turn, drives both the productivity of marine predator populations and the rate at which these populations export carbon to greater depths through excretion and deadfalls (Fig. 6c).

Discussion

Our objective in this work is to explore how the transmission and use of sensory information so evident at the resolution of individual ecological interactions[6,7,33] can influence interaction rates and, by consequence, the demography of interacting populations. Despite the diversity of ecological systems in nature, these systems exhibit important conserved features. The use of sensory information to guide motion—whether by signal-guided locomotion[12], directed growth[34] or other mechanisms[14]—is one such feature that occurs in a tremendous variety of natural systems[7]. Our analysis suggests that models of ecological dynamics may make better predictions by taking this feature into account.

One key prediction of our theory is that the relationship between interaction rate and target density will often have a sigmoid form (Fig. 2b and Extended Data Figs. 1–3). Sigmoid interaction rate functions are already widely used in ecological models, most notably as type III functional responses of the form $\lambda = a\rho^q/(1+ha\rho^q)$, where a and q are parameters that control the shape of the relationship between interaction rate and target density, and h is handling time. A major limitation of type III functional responses, however, is that the physical meaning of parameters a and q are difficult to define, and their values are not predictable a priori except in a few special cases[25,26,35]. In practice, this means that, to apply this model to any given system, one must either assume parameter values or measure them empirically[36]. In contrast, our framework derives interaction rates directly from measurable features of organismal behaviour, allowing for a priori prediction of interaction rates and their functional forms. This approach holds the promise of predicting the qualitative dynamics of coupled populations from a few key

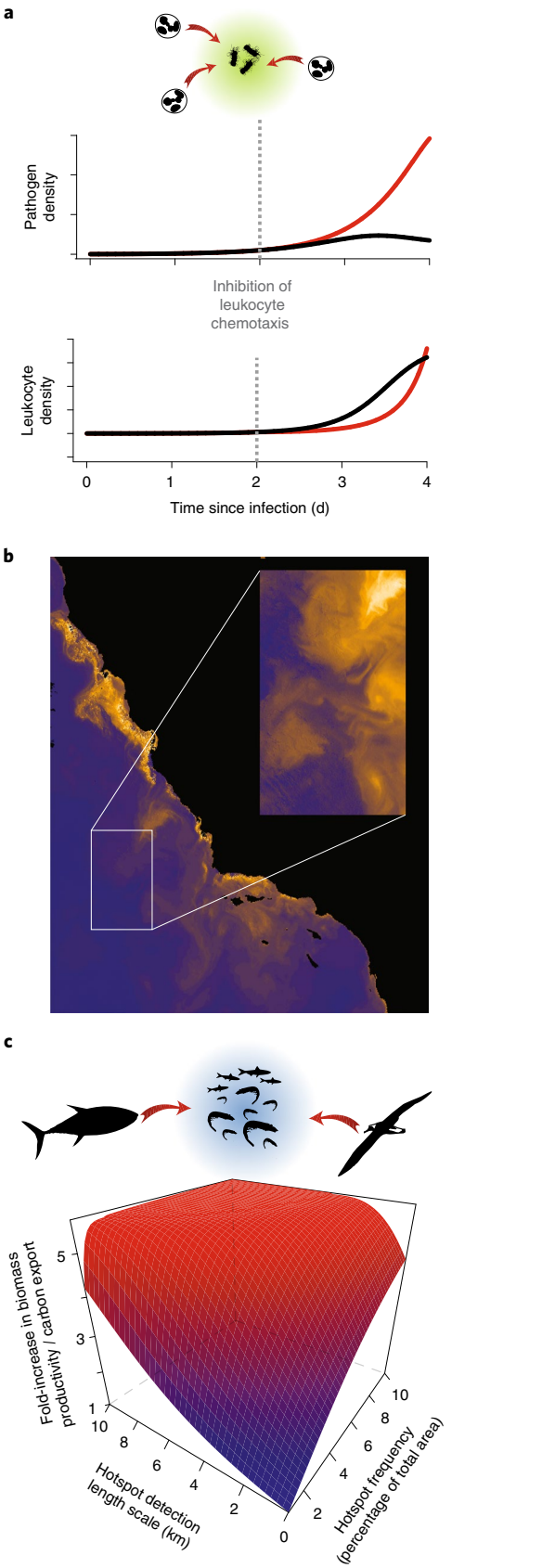

Fig. 6 | Sensory length scale drives dynamics and productivity. **a**, Pathogen infection and leukocyte dynamics during healthy immune response (black line) and response where chemotaxis is disrupted[31] (red line) at time = 2 d post-infection. Leukocytes interact with infection sites at rate $\lambda(l)$ given by information-limited kinetics[1,43]. Model details given in Methods. **b**, Chlorophyll (chl) concentration (mg chl m^{-3}, colours indicate fourth-root transformed chl concentration) in the California Current Ecosystem during the spring upwelling season (16 April 2016; data from NOAA VIIRS instrument, accessed via NOAA ERDDAP server) showing patchy productivity hotspots. Yellow indicates higher chlorophyll concentration. **c**, Factorial increase in marine predator productivity and carbon export to greater depths with change in the total extent of hotspots (% total area) and the length scale, l, over which predators can detect and move towards hotspots. Productivity computed as predator reproductive rate at equilibrium; carbon export computed as a fraction of unassimilated biomass (faecal sinking) plus a fraction of mortality (carcass sinking[5]).

functional traits that vary systematically with body size, environmental medium (for example, air and water) or sensory modality. The examples of consumer–resource dynamics (Figs. 3 and 4), host–pathogen interactions (Fig. 6a) and predator productivity in patchy environments (Fig. 6c) illustrate the power of understanding how interaction rates depend on fine-scale features of ecological interactions. Changes in the interactions themselves—for example, the changes in the length scale over which predators[32] (Fig. 4) or immune cells[31] (Fig. 6a) navigate to targets—lead to testable predictions about population dynamics.

While our framework incorporates responses of searching organisms to sensory information, there are many empirically observed features of real ecological interactions that it does not include. For example, we do not model temporal variation in predator behaviour that can occur because of changes in internal state or learning[37,38]. Other potential sources of variation in interaction rates include the particular arrangement of targets in a landscape, variability in the properties of the targets and the degree to which searchers locally deplete the landscape[14]. In the Supplementary Discussion and Extended Data Fig. 2 we present simulation results demonstrating that the major qualitative features of information limitation are preserved under a range of assumptions about target arrangement, variation in target properties and target depletion. Nevertheless, formally incorporating features like complex spatial arrangement of targets[14,39], target motion[12] and more sophisticated searcher behaviour[37,38] would provide a valuable extension to the theory of information limitation. Finally, we note that the use of sensory information to guide prey escape behaviour is another widely observed phenomenon in ecological systems[40]. While such behaviour is not explicitly incorporated into our framework, one can envision an interaction rate model that includes the ability of prey species to use sensory information to detect and evade predators. If information-driven escape behaviours affect interaction rates in a way that depends on density (for example, see ref. [41]), this phenomenon also has the potential to influence qualitative dynamics at the population scale.

The perception and use of sensory information is ubiquitous in biology. Explicitly taking this into account may significantly improve models of interacting populations, with the potential to yield insights into dynamical phenomena across ecology, physiology, oceanography and medicine.

Methods

Deriving interaction rate from searcher motion. We define an interaction as an individual instance in which a searcher and target come into physical contact. We therefore take the interaction length scale, l_i, to be on the order of one searcher body length. This covers many types of ecological interactions including the ingestion of a prey item by a predator, phagocytosis of a pathogen by an immune cell, feeding of a disease vector on a host, contact between a pollinator and a plant flower, and so forth. We define the interaction rate, λ, as the long-run rate of interactions between a single searcher and targets: $\lambda = \lim_{t\to\infty} \frac{N(t)}{t}$, where $N(t)$ is the number of targets the searcher has interacted with up to time t. By the renewal theorem, the limit converges to $\lambda = \frac{1}{E[\tau_{\text{search}} + \tau_{\text{interact}}]} = \frac{1}{\langle\tau\rangle + h}$, where τ_{search} is the time between ending one interaction and starting the next, and τ_{interact} is the duration

of interactions, $E[\cdot]$ is the expected value operator, and we have introduced the shorthand $\langle\tau\rangle := E[\tau_{\text{search}}]$ and $h := E[\tau_{\text{interact}}]$. The timescale, h, is often referred to as the handling time. Expectations are taken over many searcher–target interactions.

In conventional mean-field ecological models, searchers are considered to move independently at random through a random target landscape, either diffusively[12,13] or ballistically[11] between interactions. Under these assumptions, the interaction rate, λ, is given by mass action (that is, $\lambda \propto \rho$), when handling time, h, is negligible. This form is known as a Holling type I functional response[11]: $\lambda = \alpha\rho$, where α is a constant of proportionality. When h is non-negligible, interaction rate is given by a saturating form of mass action, $\lambda = \frac{\alpha\rho}{1+h\alpha\rho}$. This form is known as the Holling type II functional response. We use the terms 'interaction rate' and 'functional response' interchangeably throughout, but note that cases exist where they need not be equal.

Interaction rates with sensory information. In this section, we develop a model to describe interactions between searchers that move randomly at large distances and move in a target-directed fashion at distances within sensory length scale, l_* (Fig. 1a). The mean search time for this process can be divided into two components: the contribution of the random portion of the search and the contribution of the directed portion of the search.

To calculate the component of search time due to random motion (that is, $\langle\tau_{\text{random}}\rangle$) in a two-dimensional target landscape with target density, ρ, we approximate the landscape as a two-dimensional plane in which targets are located on a regular lattice with intertarget distance, $2l_o$ (refs. [13,42]). The expected time to reach a distance l_* is then computed as the mean time taken to move from a random location in the plane to within a distance l_* of one of the targets. This approach has been used to understand diffusion-limited interaction rates between molecules and cell surface receptors[42] and to model diffusion-limited interactions more generally[13,15]. The mean time to reach a distance l_* from a target is given by the solution to the backward Kolmogorov equation, $0 = 1 + D\Delta\langle\tau(x, y)\rangle$, where D is the diffusion coefficient, $\langle\tau(x,y)\rangle$ is the mean first passage time from location (x,y) and Δ is the Laplacian operator[15]. Because targets are assumed to be located on a regular lattice, a searcher that wanders out of the vicinity of one target will wander into the vicinity of another target. This suggests that the resource field can be further approximated by a circular region, with an absorbing inner boundary at l_* (within which directed search begins) and a reflecting outer boundary at radius, $l_o = (\rho\pi)^{-1/2} > l_*$ (refs. [13,42]). Because of the radial symmetry of this environment, the Kolmogorov backward equation for the first passage time to the target from any starting location, (x_0,y_0), becomes a second-order ordinary differential equation with variable coefficients and can be solved exactly. In particular, the mean time to reach l_* from initial distance, $l > l_*$ is $\frac{2l_o^2 \log\left(\frac{l}{l_*}\right) - l^2 + l_*^2}{4D}$. By integrating over all starting positions, one gets the average search time over the region of random motion, $\langle\tau_{\text{random}}\rangle$. A detailed account of how this approach can be used to solve first passage time problems is given in ref. [42].

To calculate the component of search time due to directed motion, we compute the mean time taken for searchers to reach the target from within a distance l_* of a target. For all searches that begin in the region $l > l_*$, the time to cross the region of directed search is $\frac{l-l_*}{v}$, where l_* again is the distance at which the interaction takes place. In the region $l < l_*$, the time to reach the target is $\frac{l-l_*}{v}$, where l is the initial distance to the target.

Using the above expressions for the time contributions from random and directed portions of the search, we can compute the overall mean search time and the resulting interaction rate. Assuming searches start with uniform probability over the circular region $0 < l < l_o$ leads to the equation

$$\lambda = \frac{1}{\int_0^{l_o} p(l)[\tau_{\text{random}}(l) + \tau_{\text{directed}}(l)]\,\mathrm{d}l + h} = \frac{1}{\langle\tau_{\text{random}}\rangle + \langle\tau_{\text{directed}}\rangle + h} \quad (1)$$

where

$$\langle\tau_{\text{random}}\rangle = \frac{l_o^2 - l_*^2}{l_o^2}\left[\frac{l_o^4}{2D(l_o^2 - l_*^2)}\log\left(\frac{l_o}{l_*}\right) - \frac{3l_o^2 - l_*^2}{8D}\right]$$

if $l_* < l_o$ and zero otherwise. The contribution of directed motion is

$$\langle\tau_{\text{directed}}\rangle = \frac{1}{3vl_o^2}\left[3\left(l_o^2 - l_*^2\right)(l_* - l_i) + 2l_*^3 - 3l_*^2 l_i + l_i^3\right]$$

if $l_* < l_o$. Note that $\langle\tau_{\text{directed}}\rangle$ is defined to include the contribution from searches that begin in the region $l > l_*$ and cross the region of directed motion, as well as the contribution from searches that begin within the region of directed motion $l < l_*$. In the special case where searchers move in a directed fashion throughout the environment (that is, if the length scale, l_*, is equal to or great than l_o), the expression for the contribution of directed motion simplifies to $\langle\tau_{\text{directed}}\rangle = (l_o - l_i)^2(2l_o + l_i)\left(3vl_o^2\right)^{-1}$, and there is no contribution of random motion. The dependence of equation (1) on target density, ρ, can be seen by noting that $\rho = \frac{1}{\pi l_o^2}$.

Equation (1) has a similar form to the type II functional response discussed above, with the major difference being that the 'attack rate' (that is, the inverse of the mean search time, $\frac{1}{\langle\tau\rangle} = \left[\langle\tau_{\text{random}}\rangle + \langle\tau_{\text{directed}}\rangle\right]^{-1}$), is a nonlinear function of target density, ρ. It is this nonlinearity that captures the phenomenon we refer to as information limitation.

Consumer–resource interactions, stability and collapse. Fig. 3 shows how information limitation can affect the stability and persistence of simple consumer–resource systems. To do this, we used a generalized consumer–resource model:

$$\frac{\mathrm{d}R}{\mathrm{d}t} = rR\left(1 - \frac{R}{K}\right) - \lambda(R)C$$
$$\frac{\mathrm{d}C}{\mathrm{d}t} = \lambda(R)C\varepsilon - \mu C$$

In the absence of consumers, resources grow logistically with a maximum per-capita growth rate, r, and carrying capacity, K. Consumers, eat resources at a per-capita rate $\lambda(R)$, convert consumed resources into new consumers with efficiency, ε, and die at a per-capita rate μ. When encounters between consumers and resources are governed by mass action and each interaction incurs a handling time, the model is equivalent to the Rosenzweig–MacArther consumer–resource model, where

$$\lambda(R) = \frac{aR}{1 + ahR}$$

and a is the per attack rate ($R^{-1}t^{-1}$) and h is handling time. To evaluate the role of information limitation on stability and persistence in consumer–resource systems, we evaluated consumer–resource dynamics under both mass action and information-limited kinetics (equation (1)) over a wide range of empirical parameter values (Fig. 3). For each, we solved numerically for the time-dependent dynamics of each consumer–resource system. We defined a persisting consumer–resource system as a system where neither consumer nor resource densities fell below 10^{-20} over the course of 4,000 timesteps. Fig. 3 shows the space of random consumer–resource systems explored in the analysis and the regions of parameter space where persistence occurs for the Rosenzweig–MacArthur model and the model with information-limited interaction kinetics. Additional details of model parameterizations and analysis are described in the Supplementary Discussion.

Immune cell–pathogen interactions. Changes in chemotaxis during the course of infection can be modelled using equation (1) to describe within-tissue interaction rates between a population of leukocytes and pathogen infection sites, where a disruption of chemotaxis is represented by a reduction in the length scale, l_*, during the course of the infection. We modelled dynamics using a simple coupled population model of within-tissue infection (I) and leukocytes (L) loads[1,43]:

$$\frac{\mathrm{d}I}{\mathrm{d}t} = \gamma I - \frac{L\lambda(I)}{\eta}$$
$$\frac{\mathrm{d}L}{\mathrm{d}t} = \beta + \omega L\,\lambda(I) - \delta L$$

where I is the density of the infectious population that could be either a population of infectious agents (for example, bacteria, virus or parasites) or a population of infected cells, and L is the density of leukocytes. This model posits that, in the absence of an immune response, mean infection concentration in a tissue will increase exponentially at a per-capita rate γ. Individual leukocytes encounter infectious sites at a rate $\lambda(I)$. Typically, the immune response to a local infection will involve a coordinated response by many classes of immune cells; however, for simplicity, we model a single generalized leukocyte population and assume that the elimination of a local infection requires η leukocytes to recruit to the site of the infection. Leukocytes are produced at a constant background rate β that is further stimulated by contacts with infections at rate ω and die at a per-capita rate δ. We assumed $\gamma = 2\ \mathrm{d}^{-1}$, $\eta = 100$, $\beta = 100$ cells $\mu\mathrm{l}^{-1}\mathrm{d}^{-1}$, $\omega = 1$ and $\delta = 1\ \mathrm{d}^{-1}$ to model a generic infection/immune system interaction.

Model parameters of leukocyte motion were estimated from time-lapse videos of neutrophils[20]. The parameters v (19.9 mm d^{-1}) and D (0.078 $\mathrm{mm}^2\,\mathrm{d}^{-1}$) were estimated from tracked paths of neutrophils before the initiation of chemotaxis ($t < 10$ min in Video S2 of Lämmerman et al.[20]) using the methods described in the Supplementary Discussion. We assumed $l_* = 0.1$ mm based on empirically observed immune cell responses[20,44].

Mutualistic interactions. We evaluate the effect of information limitation on the stability of mutualist population dynamics using modified Lotka–Volterra competition equations, where the sign of the interaction term is changed to model positive rather than negative interspecific interactions[45–47]. We further replace the type I functional response sometimes used in such models with a type II functional response to yield the following system of equations:

$$\frac{\mathrm{d}M_1}{\mathrm{d}t} = r_1 M_1 - m_1 M_1^2 + \zeta_1 M_1\,\lambda(M_2)$$
$$\frac{\mathrm{d}M_2}{\mathrm{d}t} = r_2 M_2 - m_2 M_2^2 + \zeta_2 M_1\,\lambda(M_2)$$

where M_1 is the density of the searcher mutualist (for example, pollinator) and M_2 is the target mutualist (for example, plant), r_i is the intrinsic growth rate of the ith species, m_i is the intraspecific competition coefficient, ξ_i governs the effect

of encounters on the growth rate of the ith species and $\lambda(M_2)$, is the functional response of the searcher mutualist species on the target species:

$$\lambda(M_2) = \frac{aM_2}{1 + ahM_2}$$

When r_1 and r_2 are both less than or equal to zero, the species are obligate mutualists[45]. We consider the special case where both r_1 and r_2 equal zero, which represents two logistically growing populations with a carrying capacity equal to zero in the absence of the other population. In this case, there is one unstable equilibrium at $M_1 = 0$, $M_2 = 0$, and one stable equilibrium where both species coexist. As long as the initial densities of mutualists are greater than zero, all populations converge to the coexistence equilibrium. However, if we replace the type II functional response with equation (1) to incorporate information limitation, the dynamics exhibit an Allee effect; the behaviour of the system depends on initial conditions as shown in Fig. 5b (red flows). If initial searcher or target densities are high, both populations will converge to a stable coexisting equilibrium, but if either initial population is too low, both populations go extinct. Under more general conditions of obligate mutualisms, where r_1 and r_2 are negative, interaction kinetics that are governed by a type II functional response can also lead to an Allee effect. In this case, replacing the type II functional response with information-limited interaction rates will generally increase the size of the basin of attraction that leads to collapse.

Marine predator biomass productivity and carbon export. To illustrate the implications of information-limited interactions in patchy environments we analysed a simple model of marine predator population dynamics and carbon cycling in a marine system containing productivity hotspots (Fig. 6b,c). To identify a relevant parameter regime, we use the California Current Ecosystem as a reference[5,48,49]. We focus on hotspots generated by frontal activity and use an estimate of 5% (1–10% range) of coastal ocean surface area classified as frontal[5]. We assumed a characteristic hotspot size, s_h, of ~10 km^2 based on the empirical range of size estimates of krill and anchovy aggregations[48]. This gives a characteristic hotspot density, $\rho_h = 5 \times 10^{-3}$ hotspots km^{-2} for the 5% hotspot area condition (range: 1×10^{-3} to 1×10^{-2} hotspots km^{-2}). We assumed that the rate of prey consumption is ten times higher in hotspots than outside hotspots due to the high density of prey in these regions and the sparsity of prey between them. This is likely to be a conservative estimate during strong upwelling conditions, where the density of prey outside hotspots can be close to zero[48]. Hotspots of the species that serve as prey for marine top predators (for example, anchovy and krill) are driven largely by aggregation and disaggregation rather than population growth; we therefore assume hotspots have a characteristic lifespan $\tau_h = 5$ d.

Within hotspots, we assume prey are dense enough that predators feed ad libitum. This can be relaxed without significantly changing our results as long as prey density within hotspots is high enough that handling time becomes the limiting factor influencing consumption rate. We set predator maximum consumption rate using the relationship $u_h = 0.1 M_C^{0.75}$ kg prey mass day^{-1} (ref. [50]), where consumer body size, M_C, is taken to be ~10 kg as representative of small marine top predators.

We consider a marine predator that detects hotspots using a physical cue such as wind-advected odours (for example, dimethyl sulfide and dimethylsulfoniopropionate[32]), sound produced at the hotspot or biosonar[51]. The length scale over which detection and directed motion towards the target becomes possible depends on the sensory modality the predator uses to detect the hotspot. Fig. 6c shows a range of values from $l_* = 0$ km to $l_* = 10$ km to cover the range of sensory modalities used by marine predators.

For the results shown in Fig. 6c, we assume that when the predator is within a distance l_* of a hotspot, it moves directly towards the centre of the hotspot. Outside hotspots, the predator moves diffusively, and the dominant motion occurs in the horizontal plane such that interactions can be modelled by equation (1). Predators feed at a rate u_h within hotspots and u_o outside hotspots. Under these assumptions, the mean rate of prey consumption by an individual predator is

$$\langle u \rangle = \frac{u_o \langle \tau_s \rangle}{\langle \tau_h \rangle + \langle \tau_s \rangle} + \frac{u_h \langle \tau_h \rangle}{\langle \tau_h \rangle + \langle \tau_s \rangle} = \frac{u_o + u_h \langle \tau_h \rangle \lambda}{1 + \langle \tau_h \rangle \lambda}$$

where we have equated the inverse of the mean search time with the patch interaction rate in the last expression: $\frac{1}{\langle \tau_s \rangle} = \lambda$. To incorporate information limitation, the interaction rate λ is given by equation (1), where a target is now taken to be a resource hotspot and l_* is the length scale over which the predator can detect and bias its motion towards the hotspot.

Population dynamics of the consumer are modelled by the equation

$$\frac{dC}{dt} = \varepsilon \langle u \rangle C - \mu C^2$$

where ε is conversion efficiency and μC^2 is a density-dependent death term. We computed long-run productivity and carbon export by solving for the consumer density at equilibrium, $C^* = \frac{\varepsilon \langle u \rangle}{\mu}$. Because at equilibrium birth and death rates are equal, the rate of production of new predator biomass is just μC^{*2}. Following ref. [5], we compute export of carbon to deeper strata as the sum of two terms: a term due to sinking of excreted unassimilated biomass that is proportional to the total population consumption rate $\varepsilon \langle u \rangle C^*$ and a term due to the sinking of dead consumers that is proportional to the total population mortality, μC^{*2}. Again, at equilibrium these two terms are proportional to one another because productivity is equal to mortality. Fig. 6c shows how productivity and carbon export rates change as a function of sensory length scale, l_*, and the fraction of the coastal ocean taken up by hotspots.

Reporting Summary. Further information on research design is available in the Nature Research Reporting Summary linked to this article.

Data availability

No data were generated in this study. Data in Fig. 1c were digitized from published studies[19,20,54–56]. Chlorophyll data shown in Fig. 6b can be freely accessed via NOAA ERDDAP server (https://coastwatch.pfeg.noaa.gov/erddap).

Code availability

Simulations and ODE system solutions were conducted in the R environment (R Development Core Team). Code is available for download as Supplementary Software.

Received: 1 May 2019; Accepted: 16 September 2019;
Published online: 28 October 2019

References

1. Nowak, M. A. & Bangham, C. R. Population dynamics of immune responses to persistent viruses. *Science* **272**, 74–79 (1996).
2. Anderson, R. M. & May, R. M. *Infectious Diseases of Humans: Dynamics and Control* (Oxford Univ. Press, 1992).
3. Suweis, S., Grilli, J., Banavar, J. R., Allesina, S. & Maritan, A. Effect of localization on the stability of mutualistic ecological networks. *Nature Commun.* **6**, 10179 (2015).
4. Levine, J. M., Bascompte, J., Adler, P. B. & Allesina, S. Beyond pairwise mechanisms of species coexistence in complex communities. *Nature* **546**, 56–64 (2017).
5. Woodson, C. B. & Litvin, S. Y. Ocean fronts drive marine fishery production and biogeochemical cycling. *Proc. Natl Acad. Sci. USA* **112**, 1710–1715 (2015).
6. Stevens, M. *Sensory Ecology, Behaviour, and Evolution* (Oxford Univ. Press, 2013).
7. Hein, A. M., Carrara, F., Brumley, D. R., Stocker, R. & Levin, S. A. Natural search algorithms as a bridge between organisms, evolution, and ecology. *Proc. Natl Acad. Sci. USA* **113**, 9413–9420 (2016).
8. Torres, L. G. A sense of scale: foraging cetaceans use of scale-dependent multimodal sensory systems. *Mar. Mammal Sci.* **33**, 1170–1193 (2017).
9. Hein, A. M., Brumley, D. R., Carrara, F., Stocker, R. & Levin, S. A. Physical limits on bacterial navigation in dynamic environments. *J. R. Soc. Interface* **13**, 20150844 (2016).
10. Nevitt, G. A. et al. Evidence for olfactory search in wandering albatross, *Diomedea exulans*. *Proc. Natl Acad. Sci. USA* **105**, 4576–4581 (2008).
11. Hutchinson, J. M. & Waser, P. M. Use, misuse and extensions of 'ideal gas' models of animal encounter. *Biol. Rev.* **82**, 335–359 (2007).
12. Dusenbery, D. B. *Living at Micro Scale: The Unexpected Physics of Being Small* (Harvard Univ. Press, 2009).
13. Gurarie, E. & Ovaskainen, O. Towards a general formalization of encounter rates in ecology. *Theor. Ecol.* **6**, 189–202 (2013).
14. Hein, A. M. & McKinley, S. A. Sensory information and encounter rates of interacting species. *PLoS Comput. Biol.* **9**, e1003178 (2013).
15. Redner, S. *A Guide to First-Passage Processes* (Cambridge Univ. Press, 2001).
16. Lanoiselée, Y., Moutal, N. & Grebenkov, D. S. Diffusion-limited reactions in dynamic heterogeneous media. *Nature Commun.* **9**, 4398 (2018).
17. Slessor, K. N., Winston, M. L. & Le Conte, Y. Pheromone communication in the honeybee (*Apis mellifera* L.). *J. Chem. Ecol.* **31**, 2731–2745 (2005).
18. McDonald, M. A., Calambokidis, J., Teranishi, A. M. & Hildebrand, J. A. The acoustic calls of blue whales off California with gender data. *J. Acoust. Soc. Am.* **109**, 1728–1735 (2001).
19. van Breugel, F., Riffell, J., Fairhall, A. & Dickinson, M. H. Mosquitoes use vision to associate odor plumes with thermal targets. *Curr. Biol.* **25**, 2123–2129 (2015).
20. Lämmermann, T. et al. Neutrophil swarms require LTB4 and integrins at sites of cell death in vivo. *Nature* **498**, 371–375 (2013).
21. Oaten, A. & Murdoch, W. W. Functional response and stability in predator–prey systems. *Am. Nat.* **109**, 289–298 (1975).
22. Rosenzweig, M. L. Paradox of enrichment: destabilization of exploitation ecosystems in ecological time. *Science* **171**, 385–387 (1971).
23. Brose, U., Williams, R. J. & Martinez, N. D. Allometric scaling enhances stability in complex food webs. *Ecol. Lett.* **9**, 1228–1236 (2006).

24. Bascompte, J., Melián, C. J. & Sala, E. Interaction strength combinations and the overfishing of a marine food web. *Proc. Natl Acad. Sci. USA* **102**, 5443–5447 (2005).
25. Murdoch, W. W. Switching in general predators: experiments on predator specificity and stability of prey populations. *Ecol. Monogr.* **39**, 335–354 (1969).
26. Real, L. A. The kinetics of functional response. *Am. Nat.* **111**, 289–300 (1977).
27. Sarnelle, O. & Wilson, A. E. Type III functional response in *Daphnia*. *Ecology* **89**, 1723–1732 (2008).
28. Williams, R. J. & Martinez, N. D. Stabilization of chaotic and non-permanent food-web dynamics. *Eur. Phys. J. B* **38**, 297–303 (2004).
29. McCauley, E., Nisbet, R. M., Murdoch, W. W., de Roos, A. M. & Gurney, W. S. Large-amplitude cycles of *Daphnia* and its algal prey in enriched environments. *Nature* **402**, 653–657 (1999).
30. Antia, R., Koella, J. C. & Perrot, V. Models of the within-host dynamics of persistent mycobacterial infections. *Proc. R. Soc. Lond. B* **263**, 257–263 (1996).
31. Reddy, R. C. & Standiford, T. J. Effects of sepsis on neutrophil chemotaxis. *Curr. Opin. Hematol.* **17**, 18–24 (2010).
32. Savoca, M. S. & Nevitt, G. A. Evidence that dimethyl sulfide facilitates a tritrophic mutualism between marine primary producers and top predators. *Proc. Natl Acad. Sci. USA* **111**, 4157–4161 (2014).
33. Cronin, T. W., Johnsen, S., Marshall, N. J. & Warrant, E. J. *Visual Ecology* (Princeton Univ. Press, 2014).
34. Cahil, J. F. & McNickle, G. G. The behavioral ecology of nutrient foraging by plants. *Annu. Rev. Ecol. Evol. Syst.* **42**, 289–311 (2011).
35. McKenzie, H. W., Lewis, M. A. & Merrill, E. H. First passage time analysis of animal movement and insights into the functional response. *Bull. Math. Biol.* **71**, 107–129 (2009).
36. Hassell, M. P., Lawton, J. H. & Beddington, J. R. Sigmoid functional responses by invertebrate predators and parasitoids. *J. Anim. Ecol.* **46**, 249–262 (1977).
37. Bartumeus, F. et al. Foraging success under uncertainty: search tradeoffs and optimal space use. *Ecol. Lett.* **19**, 1299–1313 (2016).
38. Benhamou, S. Of scales and stationarity in animal movements. *Ecol. Lett.* **17**, 261–272 (2014).
39. Raposo, E. P. et al. How landscape heterogeneity frames optimal diffusivity in searching processes. *PLoS Comput. Biol.* **7**, e1002233 (2011).
40. Cooper, W. E. Jr & Blumstein, D. T. *Escaping from Predators: An Integrative View* (Cambridge Univ. Press, 2015).
41. Gil, M. A. & Hein, A. M. Social interactions among grazing reef fish drive material flux in a coral reef ecosystem. *Proc. Natl Acad. Sci. USA* **114**, 4703–4708 (2017).
42. Berg, H. C. & Purcell, E. M. Physics of chemoreception. *Biophys. J.* **20**, 193–219 (1977).
43. Fenton, A. & Perkins, S. E. Applying predator–prey theory to modelling immune-mediated, within-host interspecific parasite interactions. *Parasitology* **137**, 1027–1038 (2010).
44. Chtanova, T. et al. Dynamics of neutrophil migration in lymph nodes during infection. *Immunity* **29**, 487–496 (2008).
45. Vandermeer, J. H. & Boucher, D. H. Varieties of mutualistic interaction in population models. *J. Theor. Biol.* **74**, 549–558 (1978).
46. Goh, B. S. Stability in models of mutualism. *Am. Nat.* **113**, 261–275 (1979).
47. Holland, J. N., DeAngelis, D. L. & Bronstein, J. L. Population dynamics and mutualism: functional responses of benefits and costs. *Am. Nat.* **159**, 231–244 (2002).
48. Benoit-Bird, K. J., Waluk, C. M. & Ryan, J. P. Forage species swarm in response to coastal upwelling. *Geophys. Res. Lett.* **46**, 1537–1546 (2019).
49. Kahru, M., Di Lorenzo, E., Manzano-Sarabia, M. & Mitchell, B. G. Spatial and temporal statistics of sea surface temperature and chlorophyll fronts in the California Current. *J. Plankton Res.* **34**, 749–760 (2012).
50. de Roos, A. M. & Persson, L. *Population and Community Ecology of Ontogenetic Development* (Princeton Univ. Press, 2013).
51. Jensen, F. H., Johnson, M., Ladegaard, M., Wisniewska, D. M. & Madsen, P. T. Narrow acoustic field of view drives frequency scaling in toothed whale biosonar. *Curr. Biol.* **28**, 3878–3885 (2018).
52. Marten, K. & Marler, P. Sound transmission and its significance for animal vocalization. *Behav. Ecol. Sociobiol.* **2**, 271–290 (1977).
53. Vergassola, M., Villermaux, E. & Shraiman, B. I. 'Infotaxis' as a strategy for searching without gradients. *Nature* **445**, 406–409 (2007).
54. Ward, S. Chemotaxis by the nematode *Caenorhabditis elegans*: identification of attractants and analysis of the response by use of mutants. *Proc. Natl Acad. Sci. USA* **70**, 817–821 (1973).
55. Dekker, T. & Cardé, R. T. Moment-to-moment flight manoeuvres of the female yellow fever mosquito (*Aedes aegypti* L.) in response to plumes of carbon dioxide and human skin odour. *J. Exp. Biol.* **214**, 3480–3494 (2011).
56. Riffell, J. A. et al. Flower discrimination by pollinators in a dynamic chemical environment. *Science* **344**, 1515–1518 (2014).

Acknowledgements

We thank members of the Information in Ecology Workshop held at UBC, S. Munch, S. McKinley, R. Nisbet, M. O'Connor, D. Brumley, F. Carrara, S. Redner and M. Gil, for comments and suggestions. A.M.H. and B.T.M. were supported by NSF IOS grant no. 1855956. A.M.H. acknowledges Simons Foundation grant no. 395890.

Author contributions

A.M.H. and B.T.M. designed the study, performed analyses and wrote the paper.

Competing interests

The authors declare no competing interests.

Additional information

Extended data is available for this paper at https://doi.org/10.1038/s41559-019-1008-x.

Supplementary information is available for this paper at https://doi.org/10.1038/s41559-019-1008-x.

Correspondence and requests for materials should be addressed to A.M.H.

Reprints and permissions information is available at www.nature.com/reprints.

Publisher's note Springer Nature remains neutral with regard to jurisdictional claims in published maps and institutional affiliations.

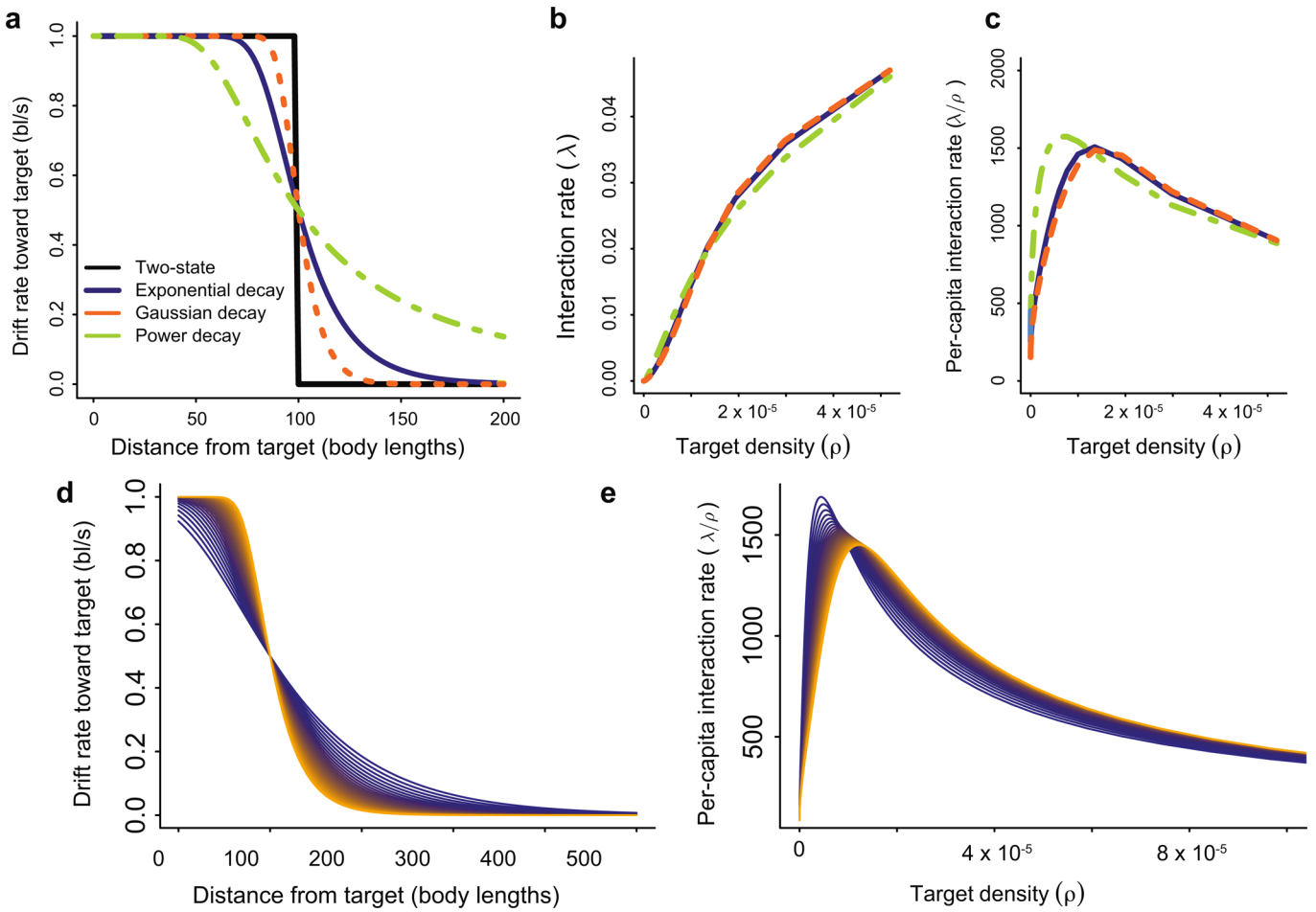

Extended Data Fig. 1 | Shape of interaction rate functions is preserved under continuous variation in the degree of directed motion. (a) Rate of drift toward target as a function of distance from the target for the two-state model described in the main text with l_*=100 body lengths (black line), and for three alternative models in which drift rate toward the target is a saturating function of a signal that decays exponentially (purple), like a Gaussian (orange) or like an inverse-square power law (green) with distance from the target. Signal decay parameters were chosen so that the mean drift speed at distance 100 body lengths are equal for all models. Drift rate, $H(l)$, is calculated as a saturating function of the signal to constrain searchers to a maximum drift speed: $H(l)=-v_{max}\tanh(S(l))$, where $S(l)$ is the signal value at a distance l, from a target (see Supplementary Discussion for details). The hyperbolic tangent form is motivated by past work on signal-dependent taxis responses[15,16]; other saturating functions yield similar results. (b) Interaction rate computed by solving Eq. (1) using the drift rates shown in panel (a). (c) Per-capita interaction rates corresponding to interaction rates shown in panel (b). Note non-monotonic form similar to that shown in Fig. 2c of the Main Text. (d) Range of drift functions with different parameter values. Each curve is one parameterization of the exponential signal function shown in panel (b) with drift rate again given by $H(l)=-v_{max}\tanh(S(l))$. Dark colored curves indicate functions in which change in drift rate with distance from target is relatively slow, whereas lighter colors are drift rate functions with more abrupt transition from high to low drift rate as distance from target increases. (e) Per-capita encounter rate as a function of target density for the same curves shown in panel (d). Note that location and height of peak changes but qualitative shape of curve is preserved.

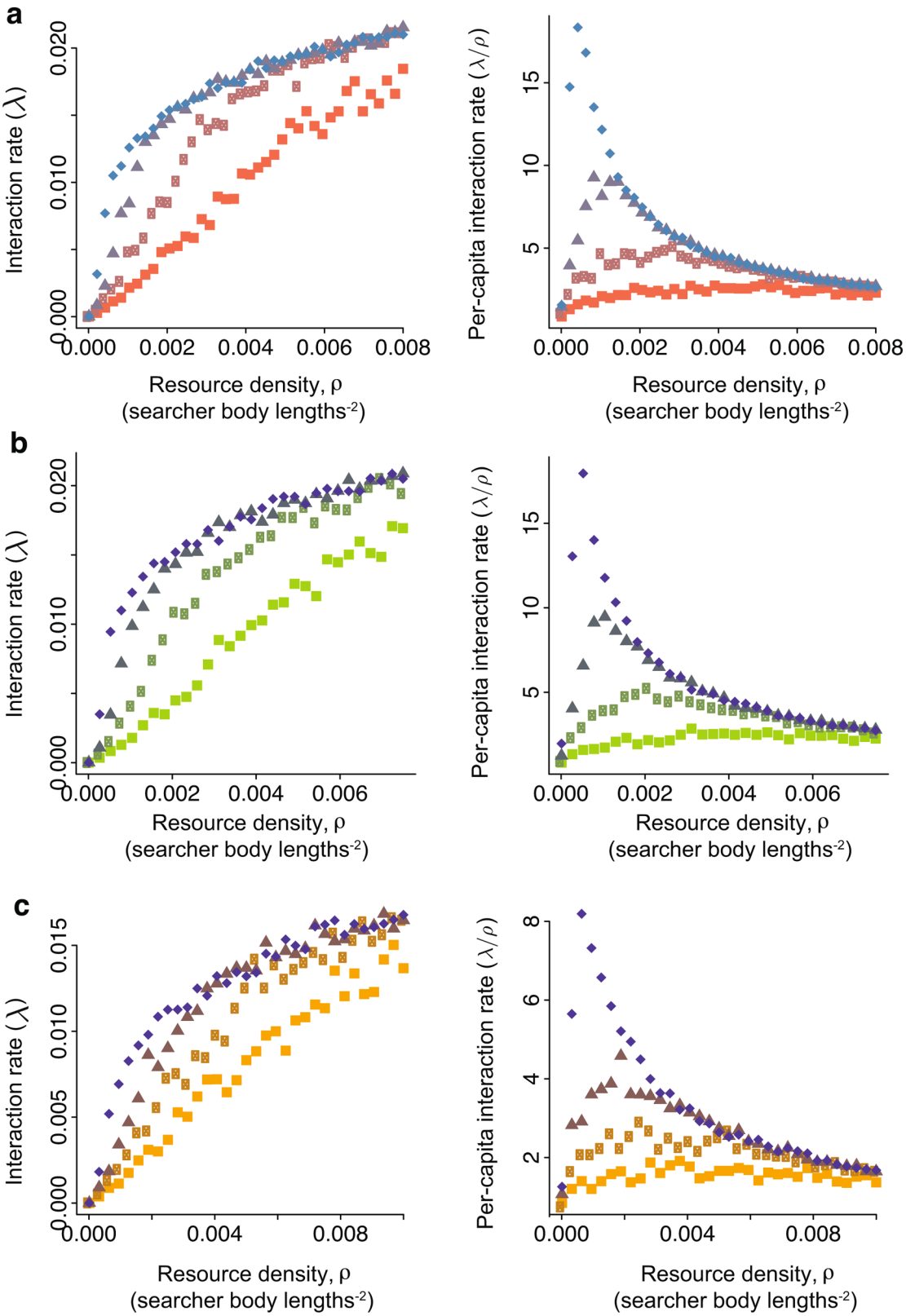

Extended Data Fig. 2 | Interaction rates in random target landscapes. (a) Interaction rate and per-capita interaction rate in a two-dimensional landscape with targets distributed according to a Poisson spatial process, (**b**) targets distributed according to a Poisson spatial process in which the length scale of sensory information, *l*., differs for each target, and (**c**) targets distributed according to a Poisson spatial process where the searcher depletes targets as it moves through the environment. Points correspond to *l*. of 5 (squares), 10 (boxes), 20 (triangles), and 40 (diamonds) body lengths. For the simulation with variable *l*., these values are averages. See Supplementary Discussion *'Robustness to spatial arrangement, target variability, and target depletion'* for a description of simulations.

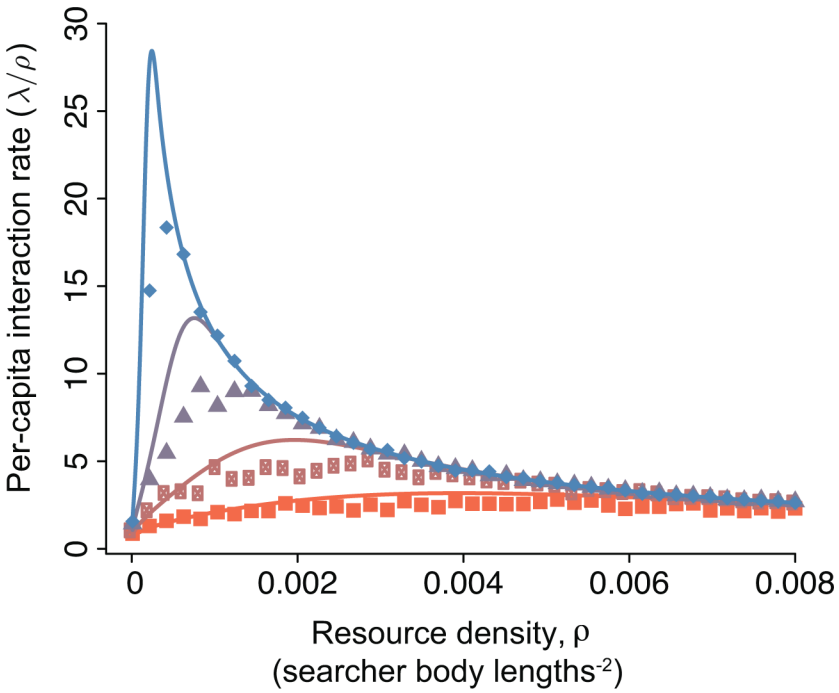

Extended Data Fig. 3 | Analytic approximation of interaction rates in a random target landscape. Per-capita interaction rates in a two-dimensional landscape with targets distributed according to a Poisson spatial process. Lines show analytic approximation (see Supplementary Discussion *'Analytic approximation for interaction rate in a random target field'*). Note that, while approximation overestimates per-capita rate at intermediate density, prediction at high and low densities is accurate, as is the predicted location of peak per-capita interaction rate.

nature research

Corresponding author(s): Andrew Hein

Last updated by author(s): 05-24-2019

Reporting Summary

Nature Research wishes to improve the reproducibility of the work that we publish. This form provides structure for consistency and transparency in reporting. For further information on Nature Research policies, see Authors & Referees and the Editorial Policy Checklist.

Statistics

For all statistical analyses, confirm that the following items are present in the figure legend, table legend, main text, or Methods section.

n/a	Confirmed
☒	☐ The exact sample size (*n*) for each experimental group/condition, given as a discrete number and unit of measurement
☒	☐ A statement on whether measurements were taken from distinct samples or whether the same sample was measured repeatedly
☒	☐ The statistical test(s) used AND whether they are one- or two-sided *Only common tests should be described solely by name; describe more complex techniques in the Methods section.*
☒	☐ A description of all covariates tested
☒	☐ A description of any assumptions or corrections, such as tests of normality and adjustment for multiple comparisons
☒	☐ A full description of the statistical parameters including central tendency (e.g. means) or other basic estimates (e.g. regression coefficient) AND variation (e.g. standard deviation) or associated estimates of uncertainty (e.g. confidence intervals)
☒	☐ For null hypothesis testing, the test statistic (e.g. *F*, *t*, *r*) with confidence intervals, effect sizes, degrees of freedom and *P* value noted *Give P values as exact values whenever suitable.*
☒	☐ For Bayesian analysis, information on the choice of priors and Markov chain Monte Carlo settings
☒	☐ For hierarchical and complex designs, identification of the appropriate level for tests and full reporting of outcomes
☒	☐ Estimates of effect sizes (e.g. Cohen's *d*, Pearson's *r*), indicating how they were calculated

Our web collection on statistics for biologists contains articles on many of the points above.

Software and code

Policy information about availability of computer code

Data collection	NA
Data analysis	Simulations and ODE system solutions were conducted using standard functions in the R statistical programming environment. Code is included as supplementary software.

For manuscripts utilizing custom algorithms or software that are central to the research but not yet described in published literature, software must be made available to editors/reviewers. We strongly encourage code deposition in a community repository (e.g. GitHub). See the Nature Research guidelines for submitting code & software for further information.

Data

Policy information about availability of data

All manuscripts must include a data availability statement. This statement should provide the following information, where applicable:

- Accession codes, unique identifiers, or web links for publicly available datasets
- A list of figures that have associated raw data
- A description of any restrictions on data availability

All data referenced in this study are available in previously published studies, which are referenced in the text and supplement. Data are used to identify plausible parameter ranges, and to illustrate how model parameters can be calculated empirically, but the central results of this study are mathematical in nature and independent of any particular dataset.

Field-specific reporting

Please select the one below that is the best fit for your research. If you are not sure, read the appropriate sections before making your selection.

☐ Life sciences ☐ Behavioural & social sciences ☒ Ecological, evolutionary & environmental sciences

For a reference copy of the document with all sections, see nature.com/documents/nr-reporting-summary-flat.pdf

Ecological, evolutionary & environmental sciences study design

All studies must disclose on these points even when the disclosure is negative.

Study description	We developed a mathematical framework to derive interaction rates between species from properties of sensing and motion. We use mathematical analyses to show how these considerations affect coupled population dynamics.
Research sample	NA
Sampling strategy	NA
Data collection	The only data used in the manuscript are from previously published studies, cited in the text or supplement. Data provide references for the relevant parameter ranges, but the main analysis is mathematical in nature and independent of data.
Timing and spatial scale	NA
Data exclusions	NA
Reproducibility	NA
Randomization	NA
Blinding	NA

Did the study involve field work? ☐ Yes ☒ No

Reporting for specific materials, systems and methods

We require information from authors about some types of materials, experimental systems and methods used in many studies. Here, indicate whether each material, system or method listed is relevant to your study. If you are not sure if a list item applies to your research, read the appropriate section before selecting a response.

Materials & experimental systems

n/a	Involved in the study
☒	☐ Antibodies
☒	☐ Eukaryotic cell lines
☒	☐ Palaeontology
☒	☐ Animals and other organisms
☒	☐ Human research participants
☒	☐ Clinical data

Methods

n/a	Involved in the study
☒	☐ ChIP-seq
☒	☐ Flow cytometry
☒	☐ MRI-based neuroimaging